Journal of Power Sources 300 (2015) 525–532

Contents lists available at ScienceDirect

Journal of Power Sources

journal homepage: www.elsevier.com/locate/jpowsour

Titanium nitride films for micro-supercapacitors: Effect of surface chemistry and film morphology on the capacitance

Amine Achour [a, b], Raul Lucio Porto [c, d], Mohamed-Akram Soussou [e], Mohammad Islam [f], Mohammed Boujtita [g], Kaltouma Ait Aissa [h], Laurent Le Brizoual [h], Abdou Djouadi [h], Thierry Brousse [h, i, *]

[a] Laboratoire d'analyse et d'architecture des systèmes (LAAS), CNRS, 7 Avenue du Colonel Roche, 31400, Toulouse, France
[b] L'ecole Nationale Polytechnique de Constantine P 75, A, Nouvelle ville RP, Constantine, Algeria
[c] Universidad Autónoma de Nuevo León, Facultad de Ingeniería Mecánica y Eléctrica, San Nicolás de los Garza, 66450, Nuevo León, Mexico
[d] Universidad Autónoma de Nuevo León, Centro de Innovación, Investigación y Desarrollo en Ingeniería y Tecnología, Apodaca, 66600, Nuevo León, Mexico
[e] LaPhyMNE, University of Gabes, Cité Erriadh, 6072, Zrig, Gabes, Tunisia
[f] College of Engineering, King Saud University, P.O. Box 800, Riyadh, 11421, Saudi Arabia
[g] CEISAM, Universite de Nantes, CNRS, 2 rue de la Houssiniere, BP 32229, 44322, Nantes Cedex 3, France
[h] Institut des Matériaux Jean Rouxel (IMN), Université de Nantes, CNRS, 2 rue de la Houssinière, BP32229, 44322, Nantes Cedex 3, France
[i] Réseau sur le Stockage Electrochimique de l'Energie (RS2E), FR CNRS, 3459, France

HIGHLIGHTS

- Titanium nitride films have been deposited with different morphologies.
- The electrode exhibits a specific capacitance in excess of 146 F cm^{-3}.
- The effect of TiN stoichiometry on film capacitance has been demonstrated.

ARTICLE INFO

Article history:
Received 16 December 2014
Received in revised form
31 July 2015
Accepted 2 September 2015

Keywords:
TiN films
Electrochemical capacitors
DC-sputtering
Porous films

ABSTRACT

Electrochemical capacitors (EC) in the form of packed films can be integrated in various electronic devices as power source. A fabrication process of EC electrodes, which is compatible with micro-fabrication, should be addressed for practical applications. Here, we show that titanium nitride films with controlled porosity can be deposited on flat silicon substrates by reactive DC-sputtering for use as high performance micro-supercapacitor electrodes. A superior volumetric capacitance as high as 146.4 F cm^{-3}, with an outstanding cycling stability over 20,000 cycles, was measured in mild neutral electrolyte of potassium sulfate. The specific capacitance of the films as well as their capacitance retentions were found to depend on thickness, porosity and surface chemistry of electrodes. The one step process used to fabricate these TiN electrodes and the wide use of this material in the field of semiconductor technology make it promising for miniaturized energy storage systems.

1. Introduction

There is an increasing demand for miniaturization and boosting the performance of the wide spread multifunctional electronic devices and micro electromechanical systems (MEMS) for more challenging and smart environments [1,2]. An integrated micro-scale power source can play a major role in device reliability and performance enhancement during operation [3], underlining the need to develop such power sources. Electrochemical capacitors, also called supercapacitors, should be suitable for on-chip integration alongside the circuit they power because of their excellent charge–discharge rate and long operating lifetime as compared to the existing micro-batteries [1]. The key issues to be addressed in developing miniaturized supercapacitors, also referred to as micro-supercapacitors, are; improvement of volumetric/areal energy density, maintaining good cycling stability and use of electrode

* Corresponding author. Institut des Matériaux Jean Rouxel (IMN), Université de Nantes, CNRS, 2 rue de la Houssinière, BP32229, 44322 Nantes Cedex 3, France.
E-mail address: thierry.brousse@univ-nantes.fr (T. Brousse).

http://dx.doi.org/10.1016/j.jpowsour.2015.09.012
0378-7753/

fabrication technique that is compatible with micro-fabrication processes [4]. Usually, powders (CNTs, activated carbon…) are processed in the form of packed films to fabricate micro-supercapacitor electrodes [5,6], a process that has many drawbacks such as bad adhesion to the current collector which adds to external resistance, loss of accessible volume to the electrolyte and incompatibility with standard micro-fabrication protocols [4]. Physical vapor deposition (PVD) techniques, widely used in the semiconductor technology manufacturing, can produce films with good adhesion, controlled thickness, composition and morphology. Thus, using PVD to fabricate electrodes for micro-supercapacitors would be the alternative solution to most of the problems faced during processing of powder into packed films. Chmiola et al. [4] have demonstrated that such technology can be used to manufacture mesoporous carbon films with high volumetric capacitance (~180 F cm^{-3}) by etching the DC-sputter deposited precursor titanium carbide film. Electrodes based on carbon materials called electrochemical double layer capacitors (EDLCs) have lower volumetric/areal energy density as compared to the so called pseudo-capacitors based on metallic oxides (RuO_2, MnO_2) [7,8] and polymeric materials [9]. Nevertheless, EDLCs are attractive as micro-supercapacitor electrodes due to long cycling life stability, thus allowing long-term use of the corresponding device.

Recently, transition metal nitrides (TMN) have been proposed as potential candidates for supercapacitors [10]. Using PVD techniques, TMN thin films such as VN [11] and RuN [12] have been proposed by our group as electrodes for micro-supercapacitors. Although these films offer high volumetric capacitance, their cycling life and power density need to be further improved for more challenging applications.

Titanium nitride (TiN) is a transition metal nitride material with remarkable properties including high electrical conductivity, high hardness and excellent thermal stability [13], making TiN films as one of the most extensively used material in semiconductor technology for electrical interconnects and diffusion barrier in MEMS devices [14]. Recently, we have demonstrated a high performance electrode for micro-supercapacitors based on TiN and carbon nanotubes (CNTs) composites (TiN/CNTs) with an outstanding cycling stability and an areal capacitance much larger than those of carbon based electrodes [15]. Producing sputter deposited TiN films as micro-supercapacitors electrode directly on a flat silicon substrates without the CNT template, while keeping performance attributes comparable to those of TiN/CNTs electrodes, will add flexibility to the design of micro-supercapacitors for practical application due to simplicity of the process and device structure as well as complementarities to EDLCs. In this work, we demonstrate that TiN, deposited on silicon substrate by reactive DC-sputtering, can be directly used as micro-supercapacitor electrodes. The volumetric capacitance value of the TiN electrodes can reach as high as 146.4 F cm^{-3} with an elegant cycling life stability of more than 20,000 cycles. Moreover, the porosity of the TiN electrode can be controlled by tailoring the deposition parameters inside the chamber during film growth, which affects both the volumetric/areal capacitance and power density of the electrodes.

2. Experimental

The TiN films were deposited over Si(100) wafers without intentional heating of the substrate holder using DC reactive magnetron sputtering technique. The deposition was carried out in a sputtering machine that is equipped with a turbo molecular pump which ensures base pressure of $<10^{-7}$ mbar in the vacuum chamber. Argon (99.999%) and nitrogen (99.999%) gases were used as sputtering and reactive gases, respectively. Titanium target (99.999%) was sputtered at different power values in order to obtain TiN films with different porosity levels and composition. The argon and nitrogen flow rates were maintained at fixed values of 18 and 2 standard cubic centimetres per minute (sccm), respectively. During deposition, the substrate holder was biased with a radio frequency generator at −75 V. A second series of TiN films, hereafter designed as T5, was prepared under similar conditions, but at a lower nitrogen partial pressure. The sample preparation conditions and their designations are summarized in Table 1. The film surface chemistry and composition as estimated by XPS, before and after in-situ erosion, are also presented in Tables 2 and 3, respectively.

Scanning electron microscope (SEM) analysis was performed using a JEOL JSM 7600 apparatus to observe morphology and to measure thickness of the deposited films. The images were recorded at an accelerating voltage of 5 kV. The films were also characterised using X-ray diffraction (XRD) machine with Bragg Brentano configuration in the range of 20–65°. Room temperature Raman spectra were recorded with a Jobin Yvon micro Raman spectrometer (T64000) at 514 nm wavelength and 200 mW power. The XPS measurements were carried out on a Kratos Axis Ultra using AlKα (1486.6 eV) radiation. High resolution spectra were acquired at 20 eV pass energy with energy resolution of 0.9 eV. The C1s line of 284.5 eV was used as a reference to correct the binding energies for charge energy shift. The Shirley background was subtracted from the spectra and signals symmetric Gaussian functions were used in the peak fitting procedure. The ellipsomertry analyses were performed using a Jobin Yvon UVISEL NIR Spectroscopic Phase Modulated Ellipsometer, with an automatic goniometer. Ellipsometric measurements were collected at an incidence angle of 70° across the spectral range 380–800 nm.

Electrochemical measurements were performed in 0.5 M K_2SO_4 (Alfa Aesar 99.99%) aqueous solution. The chemicals were used without further purification. A conventional cell with a three-electrode configuration was used for electrochemical characterization.

Electrochemical measurements were controlled via a VMP 3 multi potentiostat-galvanostat (Biologic) monitored with EC-Lab software at room temperature. A Teflon™ cell holder was used to define the surface area of the working electrode (exposed area 3 × 1 cm^2). For cyclic voltammetry experiments, ten cycles were performed prior to those provided in order to ensure that the cycles were reproducible.

3. Results and discussion

3.1. Structure and surface chemistry studies

Comparison of the XRD patterns of the T1-T4 films, shown in Fig. 1(a), indicates rock salt structure with (111) preferential orientation during films growth. The preferential orientation was found to be governed by contribution of surface energy and strain energy of the growing film. The (111) plan is known as having the lowest strain energy and the highest surface energy [16]. Therefore, it can be suggested that TiN films grew along the (111) plane in order to minimize their strain energy predominantly as a result of nitrogen excess. The XRD pattern of the T4 film was noticed to shift

Table 1
Sample identification scheme and processing conditions for TiN films.

Sample ID	T1	T2	T3	T4	T5
Power (W)	120	150	200	80	150
Nitrogen flux (sscm)	2	2	2	2	1
Argon flux (sscm)	18	18	18	18	18

Table 2
XPS analysis of the TiN films surfaces before in-situ erosion giving elemental composition.

Sample	O 1s (at. %)	Ti 2p (at. %)	N 1s (at. %)	C 1s (at. %)
T1	28.3	21.4	18.8	31.4
T2	27.4	19.6	18.7	34.4
T3	26.6	20.5	19.4	33.5
T4	38.2	22.2	17.5	30.1
T5	31.7	25.9	10.5	31.7

Table 3
Elemental composition of the TiN films from XPS studies after in-situ erosion.

Sample	O 1s (at. %)	Ti 2p (at. %)	N 1s (at. %)
T1	3.3	46.0	50.7
T2	2.5	46.5	51.0
T3	2.3	46.9	50.8
T4	19.1	39.2	41.7
T5	3.5	61.5	35.0

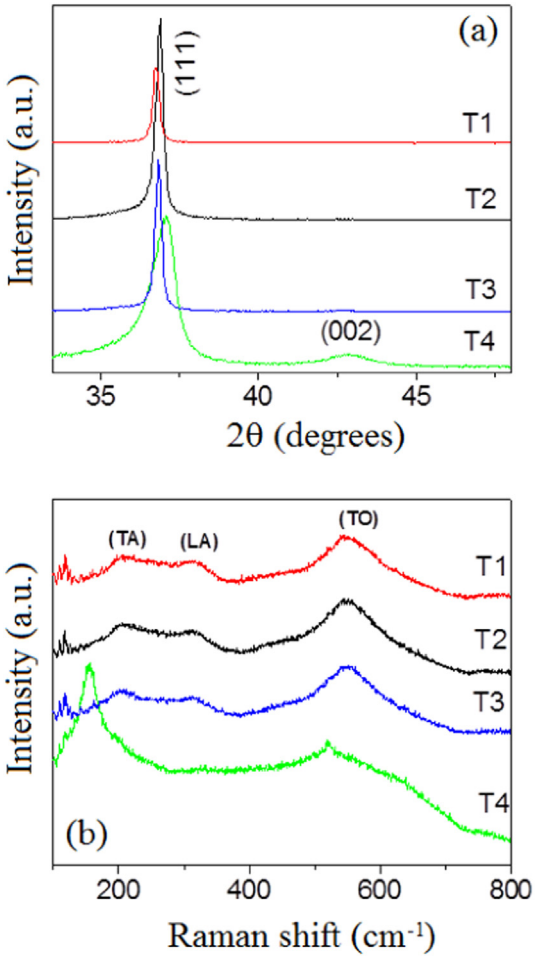

Fig. 1. (a) XRD patterns and (b) Micro-Raman spectra of T1-T4 films.

to a higher angle (by ~0.26°) with an additional orientation along (002) probably indicating towards an oxynitride film composition of TiO_xN_y rather than TiN [17]. This finding is in accordance with the XPS analysis after in-situ erosion of the deposited films (Table 3). Fig. 1(b) represents the micro-Raman spectra of the TIN films. While the spectra for the T1-T3 films are almost identical, the spectrum for the T4 film is different altogether. In the case of T1-T3 films, the low frequency peaks below 400 cm^{-1} can be attributed to acoustical phonons, whereas the high frequency mode around 540 cm^{-1} is due to optical phonons [18]. The Raman bands positioned at ~210, 310, and 515–540 cm^{-1} were identified as transverse acoustic (TA), longitudinal acoustic (LA), and transverse optical (TO) modes of δ-TiN, respectively [19]. The phonon bands in the acoustic and optic range are due to vibrations of the heavy Ti^{4+} ions and the lighter N^{3-} ions, respectively. As can be seen from Fig. 1(b), the intensity of the optical modes is higher than the acoustic part of the spectra for the samples T1-T3 suggesting that these films are over-stoichiometric (containing excess nitrogen) which is in good agreement with XPS analysis shown in Table 3. In fact, it has been shown that the optical mode intensity decreases with the decrease of N deficiency and increases with the increase of N concentration [20]. Concerning the T4 films the peaks at 153.17 and 518.5 cm^{-1} can be attributed to the vibration modes of titanium-oxynitride [21,22]. This indicates that these films contain higher amount of oxygen (as indicated in Table 3).

Surface microstructures of the T1-T4 films are displayed in SEM images, as shown in Fig. 2. It can be noticed that these films generally have a pyramidal surface morphology consisting of TiN pyramids that are single crystals with growth along (111) planar orientation and parallel to the substrate surface [23]. In fact, the sides of these pyramids are <100> family of planes which appear to impart greater roughness and larger specific area to the film surface. Furthermore, such planes are expected to provide high levels of charge storage that is accessible through minimum series resistance. The top view SEM images clearly show that the films have different degrees of apparent porosity. At a glance, it seems that the T1 film is more porous (in terms of pores density or number of pores per unit surface area) than T2 film, which in turn, is more porous than the T3 film. The porosity of T4 films also seems more important than that of the T3 film. Moreover, it can be noticed that the more porous the film is, the larger grain size is. The film thickness values measured from cross-sectional view are of the order of 670, 770, 780 and 1030 nm, respectively, for T1-T4 films.

The film porosity was assessed by ellipsometry measurements as shown in Fig. 3. The refractive index (n) can give an indication of film density and compactness. Although, n can also depend on the electronic conductivity but the similarity of surface chemistry of the films and their composition as revealed by XPS (see Table 3), allow a direct comparison of n based on the film density. Since the refractive index n_1, n_2 and n_3 of T_1, T_2, and T_3, respectively can be classified as $n_1 < n_2 < n_3$, in the visible range, one can consider that the density of these films follows the inverse evolution of n, in

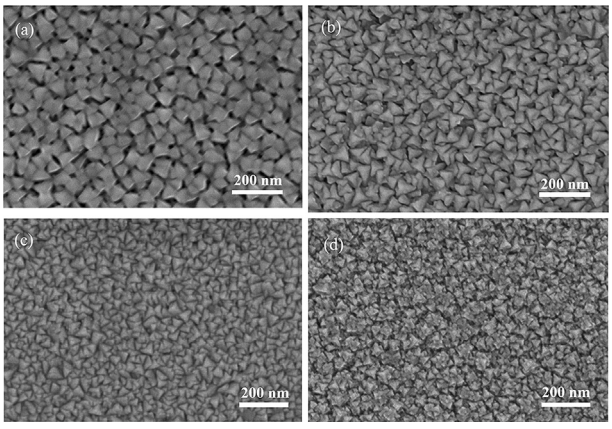

Fig. 2. Top view SEM images of (a) T1, (b) T2, (c) T3 and (d) T4 films.

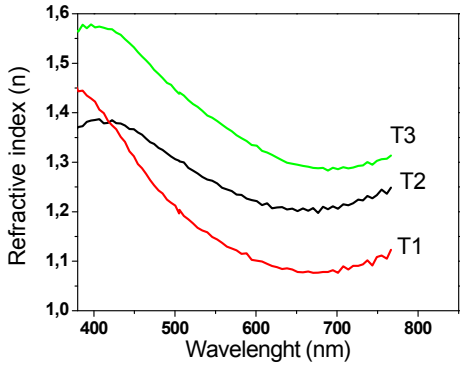

Fig. 3. Ellipsometry measurements of T1-T3 films.

accordance with SEM observations in Fig. 2. It must be noted that due to film composition difference of T_4 film compared to T_1-T_3 films, the refractive index of T_4 film can not be compared to those of T_1-T_3 films.

The TiN film produced at low nitrogen partial pressure (T5) shows different surface morphology as compared to those of T1-T4 films since the pyramidal structure is absent in this case (Fig. 4a) and the film cross-section view during SEM examination indicates columnar growth morphology with film thickness of ~1920 nm (Fig. 4b). The XRD pattern (Fig. 4c) reveals the film to be textured along (002) direction, thus indicating that the film does not contain excess nitrogen as was the case for T1-T4 films (Table 3). The micro-Raman spectrum in Fig. 4d shows presence of the same bands observed in case of T1-T3 film spectra (Fig. 1b) except that the optical mode at 540 cm^{-1} has lower intensity. This may be due to the reduced number of vibrating N^{3+} ions in the film, as inferred from XRD results, resulting in T5 film composition to be deficient in nitrogen atoms i.e. sub-stoichiometric.

The XPS high resolution Ti 2p and N1s spectra from native surfaces of the T1 and T5 films are investigated and will be presented hereafter. It should be noted that the surface chemistry of T1, T2 and T3 films is almost the same as measured by XPS analysis and only the XPS spectra of T1 and T5 films are presented and

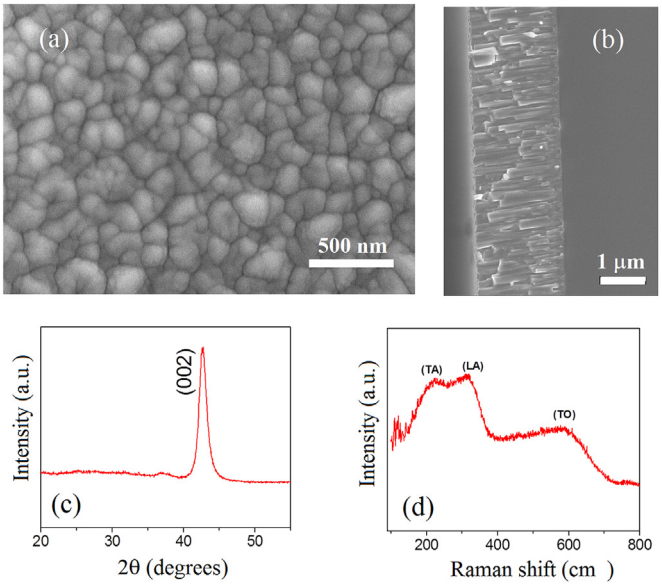

Fig. 4. (a) Top view SEM image, (b) Cross section SEM image of T5, (d) XRD diffraction pattern of T5 and (c) Micro-Raman analysis spectrum of T5 film.

compared. Significant differences in shape and position of the peaks exist between spectra of these films. The deconvolution of Ti 2p core level high resolution spectra of T1 and T5 electrodes are shown in Fig. 5a and b, respectively. The peak deconvolutions show that the T1 and T5 films exhibit major components mixture of Ti–N–O, Ti–N and Ti–O chemical bonds. In both spectra, the intense peak located at 458.2 eV can be related to Ti $2p_{3/2}$ and can be assigned to TiO_2 (Ti^{4+} oxidation state) [23] while the weaker peak at lower binding energies (~454.6 eV) can be assigned to TiN. Between these two peaks are two other peaks that can be attributed to the oxynitride (TiO_xN_y) and Ti_2O_3 which have an oxidation state between those of TiN and TiO_2 suggesting that all samples have a complex oxidized surface chemistry. The Ti 2p doublet at about 456.8 is sometimes attributed to electron energy loss induced by interaction with conduction band electrons [23,24]. However, it is believed here that this doublet can be related to Ti (Ti^{3+} oxidation state) in Ti_2O_3. At the lower energies side, the T5 sample (Fig. 5b) presents an additional weak peak that may be attributed to Ti associated with N vacancy (Ti-V_N) or, more likely, to Ti in Ti–Ti which can form in sub-stoichiomertic TiN. TiO_2 surface layer was found to have Ti_2O_3 composition beneath and the top TiO_2 layer prevents further oxidation of Ti_2O_3 to TiO_2 [25]. The Ti atom is in 3d1 configuration i.e. Ti^{3+} in the compound Ti_2O_3, a composition that is treated as an insulator with small band gap energy.

The adsorbed oxygen on the surface may diffuse inward to the bulk and substitute nitrogen to form Ti_2O_3 layer leading to N diffusion to the surface, thus giving rise to the nitrogen peak at an unusual low binding energy around 395.6 eV in the N1s spectrum, as shown in the deconvoluted N1s spectra of the T1 and T5 films (Fig. 5c and d, respectively). The peak situated in the range 396.1–396.9 eV can be attributed to titanium nitride in agreement with those of other research groups [26]. Two or three other peaks at higher energies can be resolved and may result from superposition of peaks corresponding to the oxynitride (TiN_xO_y) and nitrogen-oxygen (NO_x = NO or NO_2) or Ti-NO_x [27–30] compounds at the surface. In case of T1, one can observe an intense peak at lower energy side (395.2–395.9 eV) that may be related to some kind of nitrogen which would be negatively charged or less tightly bound such as adsorbed nitrogen, interstitial N or nitrogen associated with Ti vacancy (N–Ti_V) in the TiN sub lattice. However, this nitrogen was found to have been accumulated at the film surface, since its peak disappeared along with that of adsorbed carbon upon in-situ erosion [15]. Z. Zhang et al. [31] observed a peak at 395.9 eV, upon doping of a nano-TiO_2 powder with nitrogen through nitriding in NH_3/Ar atmosphere at temperatures in the range of 400–1100 °C, that was attributed to atomic β-N substituting oxygen in the TiO_2 sublattice and a peak at 395.5 eV that was considered as more perplexing and believed to be due to nitride in a non-ideal coordination. The peak at about 396 eV was found to be unique to $TiO_{2-x}N_x$ films. According to the literature, this peak can be assigned to atomic N substituted for oxygen sites (β-N) i.e. a chemically bound N^- state [32,33]. Moreover, it has been reported that the β-N XPS peak intensity tends to evolve along with N doping concentration [33,34]. Therefore, the observed peak at 395.5 eV in T1 film (and also in T2-T4 films) can be attributed to atomic β-N substituting oxygen in the TiO_2 sub-lattice. It has been found that TiO_2 nitrogen doping results in N 2*p* states formation within the band gap close to the valence band maximum. The associated changes in the electronic and geometric surface structure can simply be attributed to N^{3-} substituting for the lattice O^{2-} [35]. From the N 1s high resolution spectrum of T5 film (Fig. 5c), one can notice that the peak that could be related to β-N, has smaller intensity compared to those of T1-T4 films. This indicates that substitution of oxygen by nitrogen in the TiO_2 sub-lattice that forms at

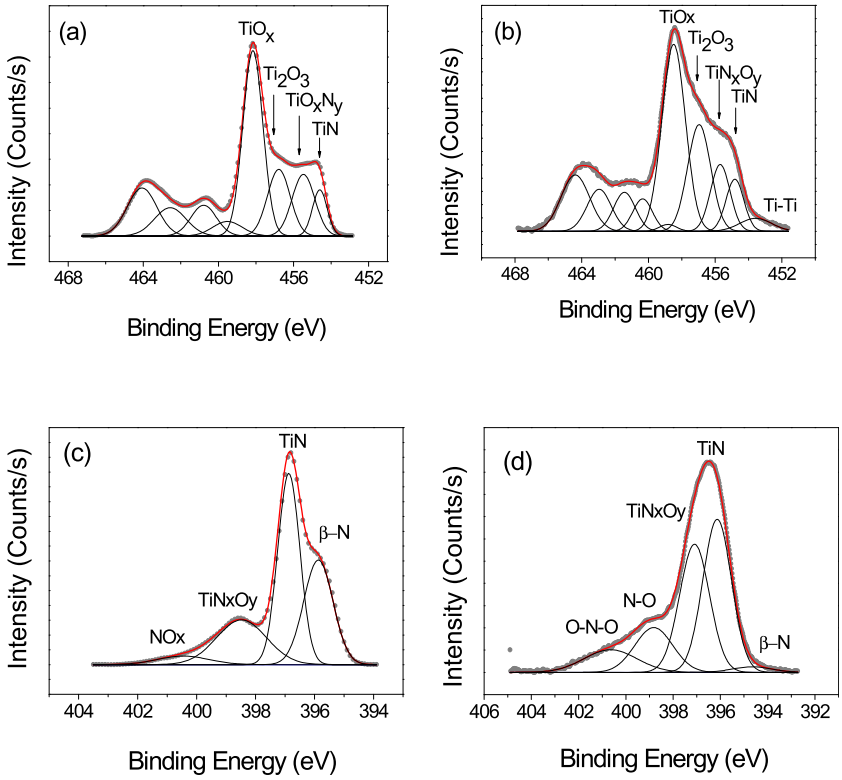

Fig. 5. (a)Ti 2p high resolution XPS spectra for T1, (b) Ti 2p high resolution XPS spectra for T5 film surfaces (c) N1s high resolution XPS spectra for T1 and (d) N1s high resolution XPS spectra for T5 surface.

the T5 surface is very low. While the TiO_2 doping, that form at the T1-T4 surfaces, with nitrogen is more important. It is must be noted that TiN at the subsurface region is the one that acts as a nitrogen source for TiO_2 doping, through nitrogen out-diffusion from the subsurface up to the surface region whereas oxygen diffusion occurs in a direction opposite to that of nitrogen [15]. Also, it was reported that N doping of TiO_2 introduces oxygen vacancies [36] which would have a role in the supercapacitive behaviour of our films, as will be described in the next section.

3.2. Electrochemical testing

Fig. 6 shows cycling voltamograms (CV) of the T1-T4 films at different scan rates. At moderate scan rates, the CV curves exhibit a nearly symmetrical rectangular shape in 0.5 M K_2SO_4 electrolyte solution, indicative of a quasi-ideal capacitive behaviour. In case of T1-T3 films, the CVs retain their rectangular shape even at high scan rate at 2 V s^{-1}. However, CV of the T4 film show less capacitive retention at scan rates higher than 50 mV s^{-1}, which may be attributed to high oxygen content in this film. As expected, the T1 film exhibits the highest capacitive retention (linear increase of current with the applied scan rate increase) where CV curves can keep their rectangular shape even at 5 V s^{-1} presumably due to larger average pore size in the film which promotes easier ions transport. Indeed, it was reported that if the average pore size is too small for cations or anions to get through, then distortion on CV occurs resulting in capacitance decrease [37]. Such high power density is comparable to that of double layer electrochemical capacitors [5,38] which is essential for micro-supercapacitors design on rigid silicon substrates. The T3 film also shows a good capacitive retention at 5 V s^{-1} even though it has low apparent average pore size compared to T1 and T2 films. This capacitive retention may be due to ions adsorption on the surface as it is shown in case of T5 films below (Fig. 8).

The volumetric and areal capacitance of the T1-T4 films as a function of scan rate are presented in Fig. 7a and b, respectively. For clarity purpose the horizontal axis of scan rate is scaled logarithmically. It should be noted that difference in the film thicknesses for T1-T3 is not considerable, especially in case of T1 and T3 films and, therefore, comparison of the areal capacitance of these films is possible. The values of volumetric and areal capacitances experience a drastic drop upon increasing the scan rate from 2 to 100 mV s^{-1}, whereas a significant capacitance level is retained over scan rates in the wide range of 0.1–5 V s^{-1}. The decrease in capacitance with scan rate increase from 2 to 100 mV^{-1} occurs not only due to the limited ion diffusion in porous electrodes but, also, due to the limitation from charge transfer rate for pseudocapacitive electrodes. The T2 film exhibits maximum volumetric (as well as areal) capacitances with values as high as 116 F cm^{-3} (corresponding to 12 mF cm^{-2}) at 2 mV s^{-1}, which is about two times higher than that of activated carbon (~40–50 F cm^{-3}) [4]. Apparently, the capacitance behaviour of TiN films follow a trend similar to that of CDC electrode [37] where the capacitance increases with decrease in pore size (T2 versus T1 films), then decreases when the pores size becomes too small for ions/cations to be able to penetrate into these pores (from comparison between T3 and T2-T1 films).

Although the carbide-derived carbon (CDC) electrodes exhibit outstanding volumetric capacitance of 160 F cm^{-3} (in H_2SO_4 electrolyte), its volumetric/areal capacitance decreases with their thicknesses increase. In our case, the film thickness increase of T1 leads to an increase of volumetric and areal capacitance as it is shown in Fig. 7b and c, respectively. For example, the volumetric capacitance increase from 15.4 up to 39.4 F cm^{-3} (at 100 mV s^{-1}) while the areal capacitance increases from 0.28 up to 8.8 mF cm^{-2} (at 100 mV s^{-1}), when the T1 film thickness increases from 180 up to 2240 nm, respectively. The increase of capacitance with film thickness increase would bring TiN films to higher level of

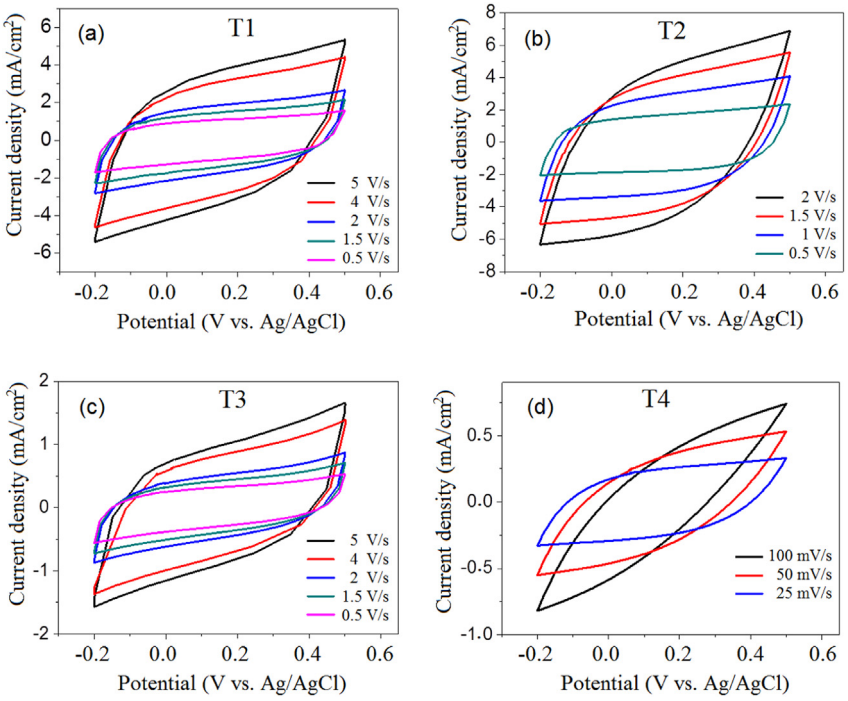

Fig. 6. Cyclic voltamograms curves versus scan rate of (a) T1, (b) T2, (c) T3 and (d) T4 films.

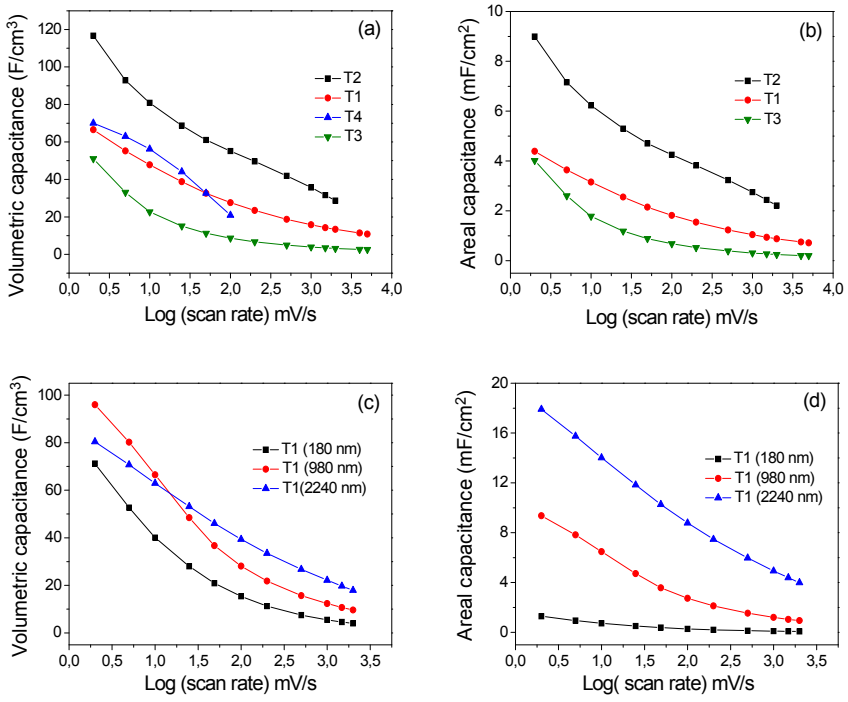

Fig. 7. (a) Comparison of volumetric capacitance of T1-T4 films versus log (scan rate) and (b) areal capacitance of T1-T3 films versus log (scan rate), (c) Volumetric capacitance and (d) areal capacitance versus log (scan rate) of 180, 980 and 2240 nm thick T1 film.

performance as micro-supercapacitors. Furthermore, an increase in the film thickness does not affect the specific capacitance of the electrodes.

At an applied potential of 0.2 V s^{-1}, the long cycling test shows excellent cycling life stability over 20,000 consecutive cycles with negligible decay in capacitance, as shown in Fig. 8a. In our previous work [15], it was suggested that this impressive stability is due to nitrogen and oxygen dynamics upon electrochemical cycling which leads to conservation of oxygen vacancy density at the electrode surface. Such cycling life stability over long-term use is crucial for micro-supercapacitor application.

The areal capacitance value of 8.8 mF cm^{-2} (at 100 mV s^{-1}) for 2240 nm thick T2 film is about three times lower than that reported for 1200 nm thick TiN-coated MWCNTs (25.5 mF cm^{-2} at 100 mV s^{-1}) in our previous work [15]. This is consistent with surface area enhancement due to the use of CNT template.

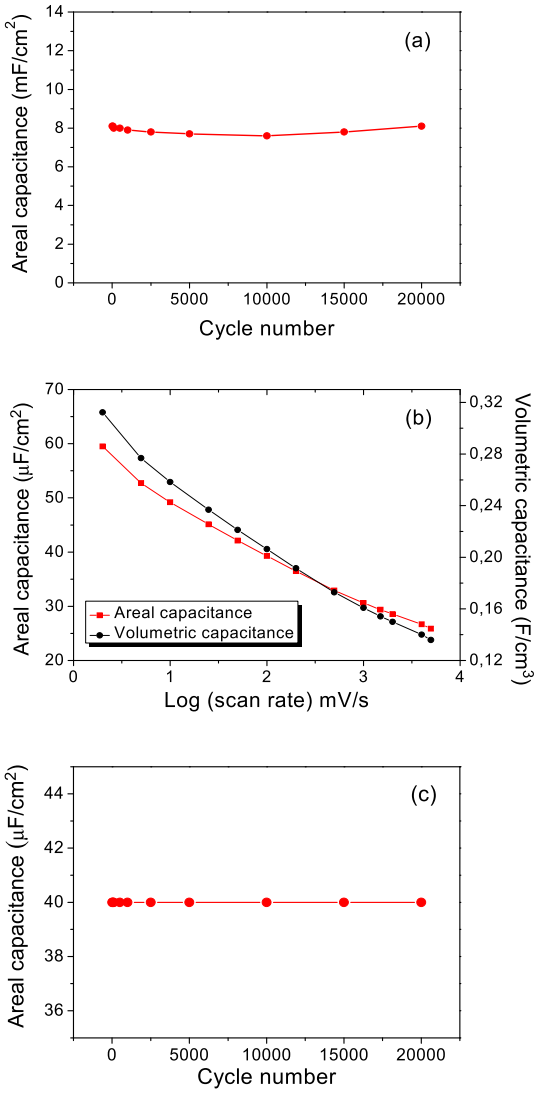

Fig. 8. (a)Cycling stability test of T1 film at scan rate of 200 mV/s, (b)volumetric and areal capacitance of T5 film at different scan rates, and (c) long cycling test at 200 mV/s.

However, in this study, we report a six-fold increase in areal and volumetric capacitances of the TiN films from 0.68 to 4.25 mF cm^{-2} (at 100 mV s^{-1}) for T2 and T4 films, respectively, without sacrificing their cycling life or power density through optimization of deposition condition. It is noteworthy that use of low-temperature (<100 °C) deposited TiN films as electrode for micro-supercapacitor electrode, without using CNT template, will reduce processing cost and facilitate the electrode integration due to simple device structure. Moreover, when compared to other pseudo-capacitive material electrodes, the obtained areal capacitance of 8.8 mF cm^{-2} at 100 mV s^{-1} is higher than that of hydrogenated TiO_2 (3.4 mF cm^{-2} at 100 mV s^{-1}) [39], NiO/TiO_2 nanotube array (2.5 mF cm^{-2} at 100 mV s^{-1}) [40] and TiO_2 nanotubes (0.9 mF/cm^2 at 2 mV s^{-1}) [41]. It is comparable to those of Ni/NiO core shell electrode (9 mF cm^{-2}) [42] and 100-nm thick MnO_2/gold hybrid electrode (12 mF cm^{-2} at 50 mV s^{1}) [43] whose cycling life is limited to few hundred cycles. The electrodes presented in this study (T1-T3) show a specific capacitance comparable to those of pseudo-capacitors but with superior cycling stability and power density.

The electrochemical evaluation of T5 film with stoichiometric or sub-stoichiometric composition is presented in Fig. 8b. The CV curves show that this film has good capacitive retention over wide range of scan rate (not shown here). The film shows remarkable cycling stability over 20,000 consecutive cycles at 200 mV s^{-1}, as shown in Fig. 8c. Nevertheless, its areal (40 μF cm^{-2} at 200 mV s^{-1}) and volumetric capacitance (0.15 F/cm^3 at 100 mV s^{-1}) values are very low as compared to T1-T4 films. The very low capacitance of T5 film, its long cycling stability and high power density are typical of EDLCs [1]. Although, the T5 film seems less porous with less surface roughness than the T1-T4 films, its very low capacitance value cannot be attributed to its average pore size only. In fact, the capacitance of the T3 film (containing smallest pores size) at 5 V s^{-1} is four times higher (200 μF cm^{-2}) than that of T5 film at 5 mV s^{-1} (50 μF cm^{-2}). It is, therefore, concluded that charge storage in the T1-T4 films is based on contributions from both double-layer and pseudo-capacitive mechanisms [15] whereas in case of T5 film, the only contribution to charge storage is made by electric double layer.

In the case of T1-T4 films, we have assumed that the N-doped TiO_2 which forms at the TiN surface (where the TiN subsurface acts as a source of β-N) leads to generation of oxygen vacancies in the TiO_2 layer and those vacancies are responsible for pseudo-capacitive contribution of charge storage in these films [15]. In case of T5 film, we believe that the pseudo-capacitive contribution is very small because an appreciable amount of oxygen vacancies in the TiO_2 layer is lacking, possibly due to absence of the β-N dopants (which generate oxygen vacancies) in T5 film, as revealed by XPS (Fig. 5b). The comparison of the surface chemistry and electrochemical properties of the T5 and T1-T3 films further supports our proposed mechanism of the charge storage in TiN [15]. These results could have implications in the design of other pseudo-capacitive materials based on transition metal nitrides.

The most important result that should be noted here is that all films which exhibit high specific capacitance are over-stoichiometric and contain appreciable quantity of β-N substituting oxygen of TiO_2 that is formed in the surface region of TiN. On the contrary, films exhibiting moderate specific capacitance are stoichiometric or sub-stoichiometric containing very low quantity of β-N or not at all. The oxygen vacancies that should form in TiO_2 as a result of N doping play a major role in charge storage mechanism in these films.

4. Conclusions

TiN films with different porosity, thickness and stoichiometry were deposited on flat silicon substrates for use as micro-supercapacitor electrodes. It has been demonstrated that the charge storage mechanism in over-stoichiometric films is due to cumulative effect of electric double layer and redox reaction. On the other hand, in case of stoichiometric or sub-stoichiometric films, the charge storage is mainly due to double layer contribution. Thus, areal and volumetric capacitance values of over-stoichiometric TiN films are much higher than that of stoichiometric or sub-stoichiometric films. Such difference in electrochemical storage behaviour is attributed to nitrogen doping of the TiO_2 layer which forms at the TiN film surface, predominantly in over-stoichiometric TiN films. The TiO_2 doping with nitrogen is believed to provoke oxygen vacancy defects which act as centres for OH^- ions adsorption. Furthermore, we have shown that over-stoichiometric films can be deposited with tailored porosity. The apparent average pore size in the films influences the capacitive storage of the films in term of specific capacitance, while high oxygen content leads to a lowering of the power density. The low synthesis temperature of our electrodes (<100 °C) will decrease the process cost and allow TiN film deposition on fragile substrates with simple device architecture. Our results can open new perspectives to explore other transition metal nitride electrodes for electrochemical storage applications.

Acknowledgements

This work was partially supported within the framework of Advanced NiBaCa project labelled by the French National Research Agency STOCK-E. The authors would like to thank J. Y. Mevellec (IMN, University of Nantes) for assistance with Raman analysis.

References

[1] P. Simon, Y. Gogotsi, Materials for electrochemical capacitors, Nat. Mater 7 (2008) 845–854.
[2] M. Armand, J.M. Tarascon, Building better batteries, Nature 451 (2008) 652–657.
[3] J.R. Miller, P. Simon, Electrochemical capacitors for energy management, Science 321 (2008) 651–652.
[4] J. Chmiola, C. Largeot, P.-L. Taberna, P. Simon, Y. Gogotsi, Monolithic carbide-derived carbon films for micro-supercapacitors, Science 328 (2010) 480–483.
[5] D. Pech, M. Brunet, P.-L. Taberna, P. Simon, N. Fabre, F. Mesnilgrente, V. Conédéra, H. Durou, Elaboration of a microstructured inkjet-printed carbon electrochemical capacitor, J. Power Sources 195 (2010) 1266–1269.
[6] T.M. Dinh, D. Pech, M. Brunet, A. Achour, High resolution electrochemical micro-capacitors based on oxidized multi-walled carbon nanotubes, J. Phys. Conf. Ser. 476 (2013) 012106.
[7] M. Toupin, T. Brousse, D. Bélanger, Charge storage mechanism of MnO_2 Electrode used in aqueous electrochemical capacitor, Chem. Mater. 16 (2004) 3184–3190.
[8] T.M. Dinh, A. Achour, S. Vizireanu, G. Dinescu, L. Nistor, K. Armstrong, D. Guay, D. Pech, Hydrous RuO_2/carbon nanowalls hierarchical structures for all-solid-state ultrahigh-energy-density micro-supercapacitors, Nano Energy 10 (2014) 288–294.
[9] G.A. Snook, P. Kao, A.S. Best, Conducting-polymer-based supercapacitor devices and electrodes, J. Power Sources 196 (2011) 1–12.
[10] D. Choi, G.E. Blomgren, P.N. Kumta, Fast and reversible surface redox reaction in nanocrystalline vanadium nitride supercapacitors, Adv. Mater. 18 (2006) 1178–1182.
[11] E. Eustache, R. Frappier, R.L. Porto, S. Bouhtiyya, J.-F. Pierson, T. Brousse, Asymmetric electrochemical capacitor microdevice designed with vanadium nitride and nickel oxide thin film electrodes, Electrochem. Commun. 28 (2013) 104–106.
[12] S. Bouhtiyya, R. Lucio Porto, B. Laïk, P. Boulet, F. Capon, J.P. Pereira-Ramos, T. Brousse, J.F. Pierson, Application of sputtered ruthenium nitride thin films as electrode material for energy-storage devices, Scr. Mater. 68 (2013) 659–662.
[13] T. Brat, N. Parikh, N.S. Tsai, A.K. Sinha, J. Poole, C. Wickersham, Characterization of titanium nitride films sputter deposited from a high-purity titanium nitride target, J. Vac. Sci. Technol. B 5 (1987) 1741–1747.
[14] L.P.B. Lima, J.A. Diniz, I. Doi, J. Godoy Fo, Titanium nitride as electrode for MOS technology and Schottky diode: alternative extraction method of titanium nitride work function, Microelectron. Eng. 92 (2012) 86–90.
[15] A. Achour, J.B. Ducros, R.L. Porto, M. Boujtita, E. Gautron, L. Le Brizoual, M.A. Djouadi, T. Brousse, Hierarchical nanocomposite electrodes based on titanium nitride and carbon nanotubes for micro-supercapacitors, Nano Energy 7 (2014) 104–113.
[16] J. Pelleg, L.Z. Zevin, S. Lungo, N. Croitoru, Reactive-sputter-deposited TiN films on glass substrates, Thin Solid Films 197 (1991) 117–128.
[17] B. Avasarala, P. Haldar, Electrochemical oxidation behavior of titanium nitride based electrocatalysts under PEM fuel cell conditions, Electrochimica Acta 55 (2010) 9024–9034.
[18] W. Spengler, R. Kaiser, H. Bilz, Resonant Raman scattering in a superconducting transition metal compound TiN, Solid State Commun. 17 (1975) 19–22.
[19] Z.H. Ding, B. Yao, L.X. Qiu, T.Q. Lv, Raman scattering investigation of nanocrystalline δ-TiNx synthesized by solid-state reaction, J. Alloys Compd. 421 (2006) 247–251.
[20] C. Chen, N. Liang, W. Tse, I. Chen, J. Duh, Raman Spectra of Titanium Nitride Thin Films, Chin. J. Phys. 32 (1994) 205–210.
[21] P. Padmavathy, R. Ananthakumar, B. Subramanian, C. Ravidhas, M. Jayachandran, Structural and electrochemical impedance spectroscopic studies on reactive magnetron sputtered titanium oxynitride (TiON) thin films, J. Appl. Electrochem 41 (2011) 751–756.
[22] X. Wu, M.-s. Zhang, Z. Yin, X. Ji, Q. Chen, Temperature characteristics of Raman spectra in nanometer material titanium dioxide, Chin. Phys. Lett. 11 (1994) 685.
[23] A. Glaser, S. Surnev, F.P. Netzer, N. Fateh, G.A. Fontalvo, C. Mitterer, Oxidation of vanadium nitride and titanium nitride coatings, Surf. Sci. 601 (2007) 1153–1159.
[24] I. leR. Strydom, S. Hofmann, The contribution of characteristic energy losses in the core-level X-ray photoelectron spectroscopy peaks of TiN and (Ti, Al)N studied by electron energy loss spectroscopy and X-ray photoelectron spectroscopy, J. Electron Spectrosc. Relat. Phenom. 56 (1991) 85–103.
[25] L. Tan, W.C. Crone, Surface characterization of NiTi modified by plasma source ion implantation, Acta Mater. 50 (2002) 4449–4460.
[26] J. Schreckenbach, F. Schlottig, D. Dietrich, A. Hofmann, G. Marx, Synthesis of cubic titanium nitride phases by anodization, J. Mater Sci. Lett. 14 (1995) 1344–1345.
[27] C. Chen, H. Bai, C. Chang, Effect of plasma processing gas composition on the nitrogen-doping status and visible light photocatalysis of TiO_2, J. Phys. Chem. C 111 (2007) 15228–15235.
[28] P. Romero-Gomez, S. Hamad, J.C. Gonzalez, A. Barranco, J.P. Espinos, J. Cotrino, A.R. Gonzalez-Elipe, Band gap narrowing versus formation of electronic states in the gap in N–TiO_2 thin films, J. Phys. Chem. C 114 (2010) 22546–22557.
[29] S.M. Prokes, J.L. Gole, X. Chen, C. Burda, W.E. Carlos, Defect-related optical behavior in surface modified TiO_2 nanostructures, Adv. Funct. Mater. 15 (2005) 161–167.
[30] X. Chen, Y.B. Lou, A.C.S. Samia, C. Burda, J.L. Gole, Formation of oxynitride as the photocatalytic enhancing site in nitrogen-doped titania nanocatalysts: comparison to a commercial nanopowder, Adv. Funct. Mater. 15 (2005) 41–49.
[31] Z. Zhang, J.B.M. Goodall, D.J. Morgan, S. Brown, R.J.H. Clark, J.C. Knowles, N.J. Mordan, J.R.G. Evans, A.F. Carley, M. Bowker, J.A. Darr, Photocatalytic activities of N-doped nano-titanias and titanium nitride, J. Eur. Ceram. Soc. 29 (2009) 2343–2353.
[32] N.C. Saha, H.G. Tompkins, Titanium nitride oxidation chemistry: an x-ray photoelectron spectroscopy study, J. Appl. Phys. 72 (1992) 3072–3079.
[33] R. Asahi, T. Morikawa, T. Ohwaki, K. Aoki, Y. Taga, Visible-light photocatalysis in nitrogen-doped titanium oxides, Science 293 (2001) 269–271.
[34] H. Matsui, H. Tabata, N. Hasuike, H. Harima, B. Mizobuchi, Epitaxial growth and characteristics of N-doped anatase TiO2 films grown using a free-radical nitrogen oxide source, J. Appl. Phys. 97 (2005).
[35] M. Batzill, E.H. Morales, U. Diebold, Influence of nitrogen doping on the defect formation and surface properties of TiO_2 rutile and anatase, Phys. Rev. Lett. 96 (2006) 026103.
[36] A.K. Rumaiz, J.C. Woicik, E. Cockayne, H.Y. Lin, G.H. Jaffari, S.I. Shah, Oxygen vacancies in N doped anatase TiO_2: experiment and first-principles calculations, Appl. Phys. Lett. 95 (2009).
[37] M. Heon, S. Lofland, J. Applegate, R. Nolte, E. Cortes, J.D. Hettinger, P.-L. Taberna, P. Simon, P. Huang, M. Brunet, Y. Gogotsi, Continuous carbide-derived carbon films with high volumetric capacitance, Energy & Environ. Sci. 4 (2011) 135–138.
[38] F. Wei-Chuan, C. Kuei-Hsien, C. Li-Chyong, Superior capacitive property of RuO_2 nanoparticles on carbon nanotubes incorporated with nitrogen, Nanotechnology 18 (2007) 485716.
[39] X. Lu, G. Wang, T. Zhai, M. Yu, J. Gan, Y. Tong, Y. Li, Hydrogenated TiO_2 nanotube arrays for supercapacitors, Nano Lett. 12 (2012) 1690–1696.
[40] J.-H. Kim, K. Zhu, Y. Yan, C.L. Perkins, A.J. Frank, Microstructure and pseudocapacitive properties of electrodes constructed of oriented NiO-TiO_2 nanotube arrays, Nano Lett. 10 (2010) 4099–4104.
[41] M. Salari, K. Konstantinov, H.K. Liu, Enhancement of the capacitance in TiO_2 nanotubes through controlled introduction of oxygen vacancies, J. Mater. Chem. 21 (2011) 5128–5133.
[42] J.-H. Kim, S.H. Kang, K. Zhu, J.Y. Kim, N.R. Neale, A.J. Frank, Ni-NiO core-shell inverse opal electrodes for supercapacitors, Chem. Commun. 47 (2011) 5214–5216.
[43] X. Lang, A. Hirata, T. Fujita, M. Chen, Nanoporous metal/oxide hybrid electrodes for electrochemical supercapacitors, Nat. Nano 6 (2011) 232–236.